

Valorization of Industrial Wastes for the Production of Glass–Ceramics

Anna Kritikaki¹ · Dimitra Zaharaki¹ · Kostas Komnitsas¹

Received: 14 September 2015 / Accepted: 10 January 2016 / Published online: 14 January 2016
© Springer Science+Business Media Dordrecht 2016

Abstract In the present experimental study, the valorization potential of various industrial wastes, namely fly ash, red mud and ferronickel slag was investigated for the production of CaO–Al₂O₃–Fe₂O₃–SiO₂ glass–ceramics. Glass was first produced in alumina crucibles at 1300 and 1500 °C and then cast in stainless steel moulds. After cooling, glass was pulverized, uniaxially pressed at 60 MPa and used for the production of glass–ceramics in the form of disks. The chemical composition of glass and the sintering temperature affected the properties, namely microstructure, porosity, compressive strength, Vickers microhardness and linear thermal expansion coefficient of the produced glass–ceramics. The leaching potential of hazardous elements present in glass–ceramics was investigated with the Toxicity Characteristics Leaching Procedure test, their chemical stability was evaluated through immersion of specimens in distilled water, simulated acid rain solution and seawater for a maximum period of 1 month, while their structural integrity was assessed according to ASTM standard C1262-10. Several analytical techniques, namely X-ray Diffraction, Scanning Electron Microscopy, Differential Thermal Analysis and Fourier Transform Infrared Spectroscopy (FTIR) were used to provide insights on the microstructure of the produced glass–ceramics.

Keywords Glass–ceramics · Industrial waste · Fly ash · Red mud · Ferronickel slag

Introduction

Valorization of industrial wastes, especially those produced in huge quantities, is today a matter of very high industrial and social importance by taking into account the principles of circular economy and environmental protection [1]. Vitrification, which aims at immobilization of pollutants in a matrix with high chemical stability, is one of the proven technologies for the management of non-combustible hazardous industrial wastes [2].

If the industrial wastes contain glass forming constituents (CaO, SiO₂, Al₂O₃ and Fe₂O₃) they can be transformed into glassy materials. These waste-based glasses can then be transformed into glass–ceramics [3]. Glass–ceramics are fine grained polycrystalline materials, which are produced after controlled crystallization of a parent glass and may also have a residual glass matrix. They may exhibit superior mechanical properties compared to the parent glass, as well as very good thermal and electrical properties and resistance to erosion [4, 5].

The first attempts for the production of glass–ceramics from industrial wastes are dated back to the 70s. Since then several waste types have been examined and glass–ceramics with superior properties have been produced after utilization of ashes from thermal power plants [6–12] and waste incinerators [13–16], other industrial and municipal [17–22] and even radioactive wastes [23, 24]. Glass–ceramics can be used as construction materials [25–28], filters and membranes [29–31], catalytic supports [32, 33] and sensors [34–36].

Glass–ceramics may also be produced after mixing industrial wastes with several other by-products having favorable composition. Barbieri et al. [37] have shown that glasses and glass–ceramics with improved mechanical properties can be obtained by mixing up to 50 wt% of

✉ Dimitra Zaharaki
zaharaki@mred.tuc.gr

¹ School of Mineral Resources Engineering, Technical University Crete, 73100 Chania, Crete, Greece

Italian or Spanish coal fly ash (CFA) with other wastes (glass cullet and float dolomite). Also, glass–ceramics produced from mixtures of fly ash, peat, clay and waste glass exhibited high relative density (2.4 g/cm^3) and mechanical strength (72 MPa) [38].

However, the main drawback for the production of glass–ceramics from industrial wastes is the high temperature required for melting of glass. In order to substantially reduce melting temperature and thus the associated production cost, several approaches were considered by mixing materials of different compositions. Thus, industrial wastes including slags, red mud, galvanic glass microspheres, acid neutralization salts and medical wastes can be mixed with or without the addition of natural raw materials, e.g. clay, alumina–silicon carbide and silica sand to produce more economically glass–ceramics with adequate physical and mechanical properties (e.g. compressive strength as high as 80 MPa) and low content of hazardous elements [39, 40].

In the present study, high calcium fly ash, red mud and low calcium ferronickel slag were mixed for the production of $\text{CaO-Al}_2\text{O}_3\text{-Fe}_2\text{O}_3\text{-SiO}_2$ glass–ceramics. The objectives of the study were (i) the production of useful products by reusing wastes produced in enormous quantities worldwide and (ii) the stabilization of toxic and hazardous elements that are present in the initial wastes. Four different binary compositions were tested and the effect of mineralogy and sintering temperature on the properties of the produced glass–ceramics was investigated.

Experimental Design

Raw Materials

The raw materials used in the present study were: (i) fly ash obtained from the thermal power plant of Ptolemais, NW Greece, (ii) red mud obtained from “Aluminum of Greece” plant, Agios Nikolaos, prefecture of Veotia, Greece and (iii) electric arc furnace slag obtained from the “LARCO S.A” ferronickel plant, Larymna, prefecture of Lokris, Greece. Table 1 shows the chemical composition of the raw materials used in the form of oxides and trace elements, as derived from an X-ray fluorescence energy dispersive spectrometer (XRF-EDS) Bruker-AXS S2 Range Type. Loss on ignition (LOI) was determined by heating raw materials at $1050 \text{ }^\circ\text{C}$ for 4 h.

X-ray Diffraction (XRD) analysis of the raw materials, as well as of glasses and glass–ceramics, was carried out using a Bruker AXS (D8 Advance type) diffractometer with a $\text{Cu-K}\alpha$ radiation and a scanning range from 4° to $70^\circ 2\theta$, with step 0.02° and 0.2 s/step measuring type. Qualitative analysis was performed using the DIFFRAC plus

Table 1 Chemical composition (% w/w) of raw materials

Component	Fly ash	Red mud	Slag
$\text{Fe}_2\text{O}_{3(\text{tot})}$	5.6	41.65	43.83
SiO_2	33.4	9.28	32.74
Al_2O_3	13.1	15.83	8.32
CaO	31.85	10.53	3.73
MgO	3.67	1.13	2.76
MnO	0.18	–	0.41
Na_2O	0.46	2.26	–
K_2O	0.76	0.21	–
P_2O_5	–	0.12	–
TiO_2	0.71	4.73	–
SO_3	6.58	0.3	0.45
Cr_2O_3	0.06	0.09	3.07
C	–	–	0.11
Ni (mg/kg)	460	1055	1000
Co (mg/kg)	68	–	200
LOI	2.7	12.77	–
Total	99.13	99	95.54

EVA v. 2006 software and the Powder Diffraction File (PDF-2) database.

The fly ash used in the present study is classified as class C ($\text{SiO}_2 + \text{Al}_2\text{O}_3 + \text{Fe}_2\text{O}_3 > 50 \%$), while the main crystalline phases detected by XRD are portlandite, anorthite, calcite and quartz. Red mud is a by-product of alumina production by the Bayer process, and its volume and composition may vary widely depending on the type of bauxite treated. Red mud consists mainly of iron and aluminum oxides. Ferronickel slag consists of forsterite and fayalite (olivines), quartz, anorthite and cristobalite while its amorphous content exceeds 50 %. Commercial silica sand with 98 % purity, purchased from Athens, Greece, was also used in some tests.

All materials were ground prior to use using a FRITSCH pulverizer (Germany) and the average particle size was determined by laser particle analysis using a MASTERSIZER S, Malvern Instrument. The mean particle size of the raw materials used for the production of glasses varied from 30 to $45 \mu\text{m}$, while for the production of glass ceramics the mean particle size of glasses varied between 30 and $80 \mu\text{m}$.

Synthesis of Glasses

The binary compositions and the experimental conditions used for the synthesis of glasses are shown in Table 2. The presence of fly ash and silica sand enhances the glass forming ability of the mixtures while red mud and slag, with Fe_2O_3 content 41.65 and 43.83 % respectively, act as

Table 2 Binary compositions and experimental conditions used for glass synthesis

Composition	PFA (%)	RM (%)	SK (%)	SS (%)	Borax/sodium carbonate (%)	Temperature (°C)
50P50RM	50	50	–	–	–	1500
90P10RM	90	10	–	–	–	1500
90P10SS	90	–	–	10	10/10	1500
90P10SK	90	–	10	–	10/10	1300

PFA ptolemais fly ash, RM red mud, SS silica sand, SK slag

a source of Fe which lowers the melting temperature of glass.

In order to decrease both the melting temperature of the mixture and the viscosity of the produced molten glass, 10 % w/w of borax (Sigma Aldrich, Germany) and 10 % w/w of sodium carbonate (Fluka, Germany) were also added in two cases. Glasses were produced in alumina crucibles after heating the mixtures for 2 h at 1300 or 1500 °C. Molten glasses were cast in stainless steel moulds.

Glasses were analyzed by Differential Thermal Analysis (DTA) to elucidate the crystallization process and determine both glass transition (T_g) and crystallization peak temperature (T_c). DTA analysis was performed using a Perkin Elmer Pyris DTA/TG analyzer, while samples were heated from 40 to 1200 °C with a constant rate of 10 °C/min.

Synthesis of glass–ceramics

The pulverized glasses were used as raw materials for the production of glass–ceramics. Four different glass–ceramics were prepared in disks and uniaxially pressed at 60 MPa (sample dimensions ϕ 30 mm diameter, h ~ 15–25 mm). The use of pulverized materials improves processing and the functional characteristics of the final products.

The green samples were dried at 110 °C and then sintered for 2 h at temperatures varying between 800 and 1000 °C, using a heating rate of 3 °C/min. Open porosity and bulk density of the glass–ceramics were determined by mercury porosimetry (Micromeritics Autopore IV 9500); measurements were done in triplicate. The standard deviation in all cases was less than 5 %. The compressive strength was determined as the average of three measurements using an MTS 800 load frame. Vickers microhardness measurements were taken using a FM-800 Future-Tech microhardness tester. Samples were polished using diamond paste and a load of 500 g was applied. To obtain reproducible results 10 indentations were made on each sample. Dilatometric studies on glass–ceramics produced after sintering at 900 °C were also performed to determine

the coefficient of thermal expansion (CTE) between 40 and 600 °C using a Netzsch DIL 402C dilatometer.

The functional groups present in glass–ceramics were identified through FTIR analysis using KBr pellets in a Perkin Elmer Spectrum 1000 spectrometer; each sample was mixed with KBr at a ratio 1:100 w/w and pressed to obtain a disc. The microstructure of the glass–ceramics was determined by Scanning Electron Microscopy (SEM) using a JEOL 6380LV scanning electron microscope equipped with an EDS INCA microanalysis system. Samples were mounted in resin and then thin polished sections were prepared.

The toxicity of glass–ceramics was investigated by using the TCLP (Toxicity Characteristics Leaching Procedure) test [41]. The concentration of Cr, Ni, Zn, Cd, Pb and Cu in the extract was determined using an Agilent Technologies 7500cx inductively coupled plasma mass spectrometry (ICP-MS) analyzer (Agilent Technologies, Santa Clara, CA, USA).

The chemical stability of glass–ceramics was investigated through immersion of specimens in distilled water, simulated acid rain ($H_2SO_4:HNO_3$ 60:40 % w/w, pH 3) and seawater for 1, 7 days and 1 month. After immersion for the predefined period the specimens were weighted and the weight loss was calculated. Weight loss was calculated in each case as the average of 5 measurements. The structural integrity of the specimens was assessed by employing two 48 h freeze–thaw cycles, with –10 and 80 °C as temperature extremes, according to ASTM standard C1262-10. Weight loss and compressive strength have been also determined after the end of the tests.

Results and Discussion

Composition of Glass–Ceramics

Glasses were initially prepared and chemically characterized as shown in Table 3 in order to elucidate the effect of their composition on microstructure and properties of the produced glass–ceramics. The XRD patterns of glass and glass–ceramics produced after sintering of the glass powder at different temperatures are presented in Figs. 1, 2, 3, 4.

Table 3 Chemical composition (w/w %) of glasses

	G-90P10SS	G-90P10SK	G-50P50RM	G-90P10RM
Fe ₂ O ₃	4.13	16.15	24.18	6.81
CaO	15.90	15.14	22.31	19.03
Al ₂ O ₃	6.16	8.27	22.81	18.93
SiO ₂	46.96	26.53	15.94	35.91
TiO ₂	0.42	0.71	3.16	1.53
MgO	1.96	3.70	1.74	2.14
Na ₂ O	9.22	6.32	0.13	0.52
P ₂ O ₅	0.10	0.07	0.15	0.14
SO ₃	0.85	0.33	0.00	0.15
K ₂ O	0.96	0.73	0.61	1.24
MnO	0.01	0.15	0.05	0.03
NiO	0.01	0.04	0.05	0.02
CuO	–	–	–	0.01
ZnO	–	0.01	0.01	–

The patterns indicate that when the sintering temperature increases from 800 to 1000 °C more crystalline phases are developed, while the amorphous content of glass–ceramics, which is indicated by the wide shoulder shown between 17° and 38°, is reduced. Figure 1 shows that addition of 10 % w/w silica sand in fly ash for the synthesis of glass (G-90P10SS) results in the formation of diopside, feldspars, brownmillerite and spinel (chromite) in the respective glass–ceramic (GC-90P10SS). At the highest sintering temperature (1000 °C) the peaks of feldspar and brownmillerite become stronger. Brownmillerite, which is a calcium ferrite, is formed from the reaction of CaO and Fe₂O₃ at temperatures approaching 1000 °C and may also exhibit catalytic properties [42].

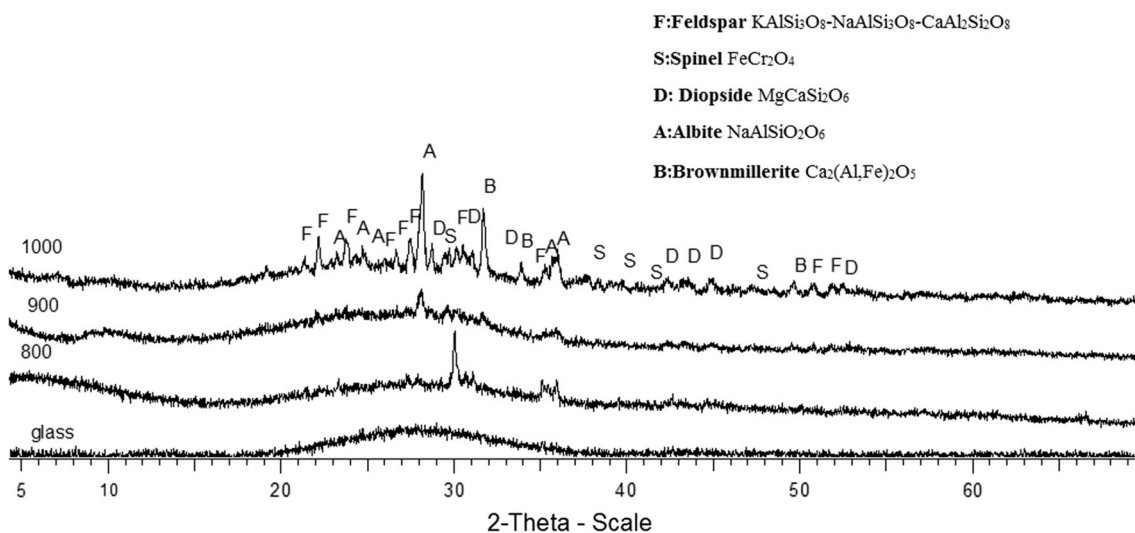
Sintering of glass produced from fly ash and 10 % w/w slag (G-90P10SK) results among others in the formation of nepheline, brownmillerite, gehlenite, spinel and hematite in the respective glass–ceramic (GC-90P10SK) (Fig. 2). The intensity of brownmillerite, spinel and hematite peaks increases with increasing sintering temperature. It is known that when the sintering temperature exceeds 800 °C partial decomposition of spinels takes place. This decomposition may be aided by chlorite which is present in fly ash [43].

Figures 3 and 4 show the XRD patterns of glass–ceramics (GC-50P50RM, GC-90P10RM) as well as of the initial glasses (G-50P50RM and G-90P10RM), formed from fly ash and red mud. It is shown that in the GC-90P10RM glass–ceramic, which is formed from glass produced mainly from fly ash, the peaks of gehlenite, albite and wollastonite exhibit high intensity. This is due to the fact that fly ash has much higher content of SiO₂ and CaO compared to red mud (Table 1). On the other hand the presence of hematite in glass–ceramic GC-50P50RM is due to the increased content of Fe in red mud, the raw material used in 1:1 ratio with fly ash for the synthesis of the respective glass G-50P50RM [44, 45].

Microstructure of Glass–Ceramics

Figure 5 shows SEM images and the respective element spectra as derived through EDS analysis of glass–ceramics produced after sintering of glasses formed at 900 °C.

It is shown that in all glass–ceramics crystals of different size and shape are distributed within the glassy phase. In glass–ceramics produced after sintering of glass formed from fly ash and silica sand (GC-90P10SS), few pores with irregular shapes are visible (Fig. 5a). EDS analysis

**Fig. 1** XRD patterns of glass G-90P10SS and the produced glass–ceramic GC-90P10SS at 800, 900 and 1000 °C

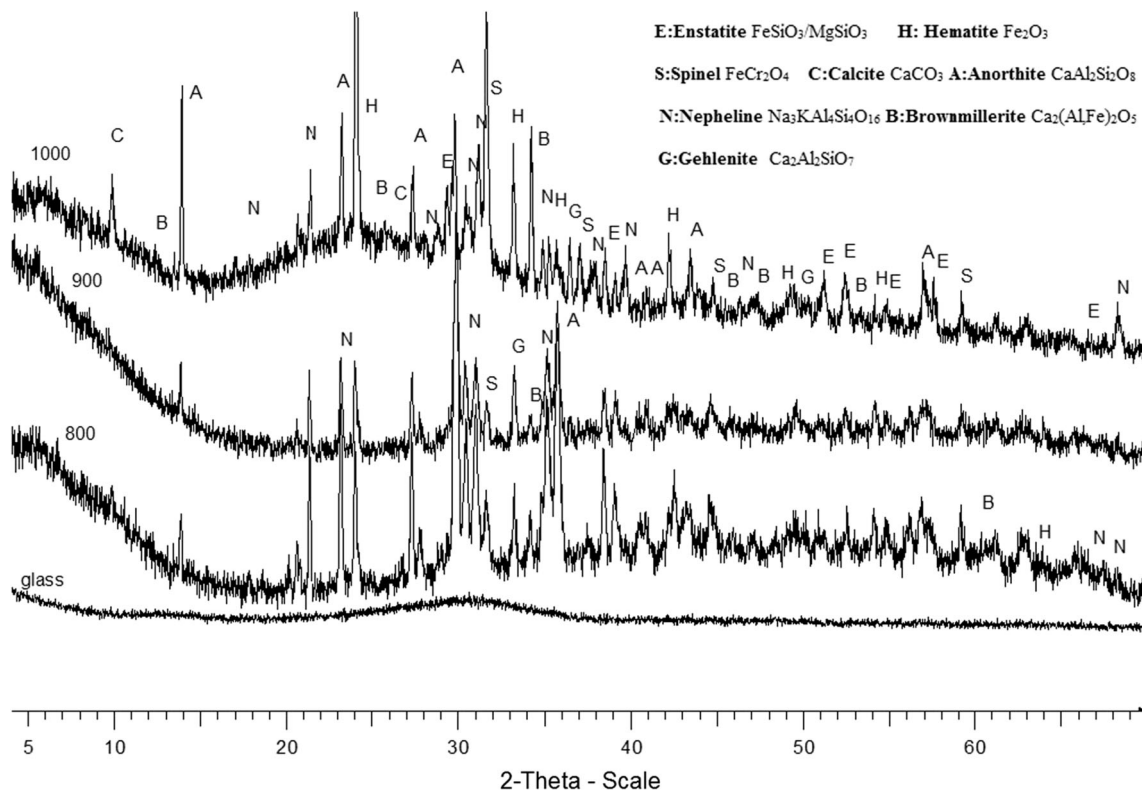


Fig. 2 XRD patterns of glass G-90P10SK and the produced glass–ceramic GC-90P10SK at 800, 900 and 1000 °C

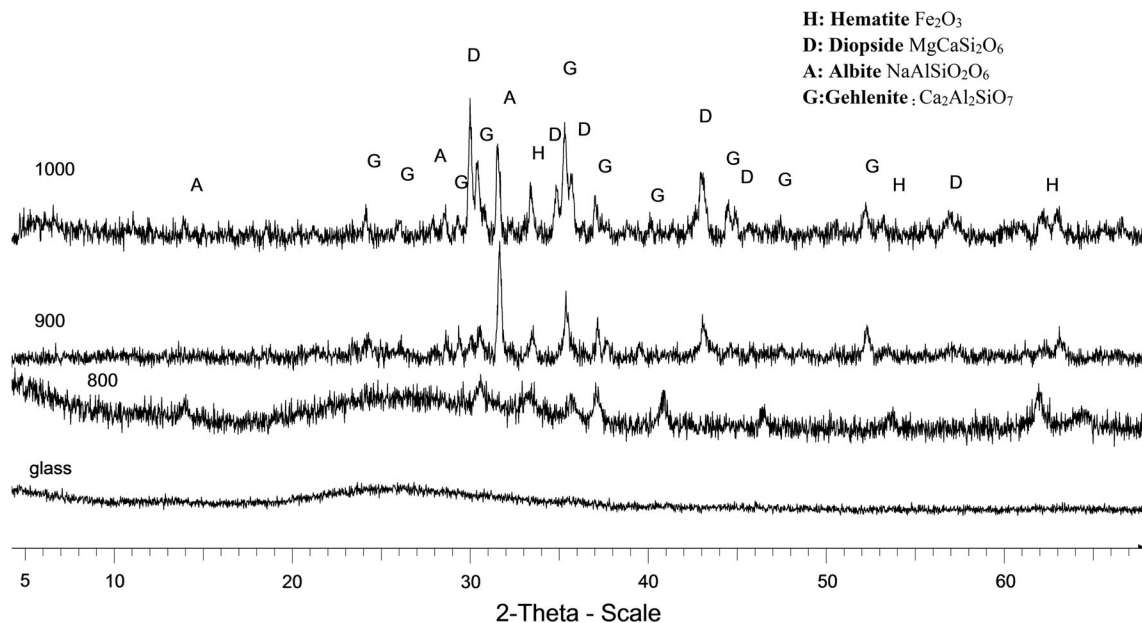


Fig. 3 XRD patterns of glass G-50P50RM and the produced glass–ceramic GC-50P50RM at 800, 900 and 1000 °C

indicates the presence of phases such as chromite and diopside (Fig. 5b) as well as the glassy phase (Fig. 5c).

Figure 5d shows the microstructure of glass–ceramics produced after sintering of glass produced from fly ash and

10 % red mud (GC-90P10RM). In this glass–ceramic a big number of pores with irregular shape is seen (Fig. 5e). Needle shape wollastonite crystals forming a dendritic network are uniformly dispersed within the glassy phase.

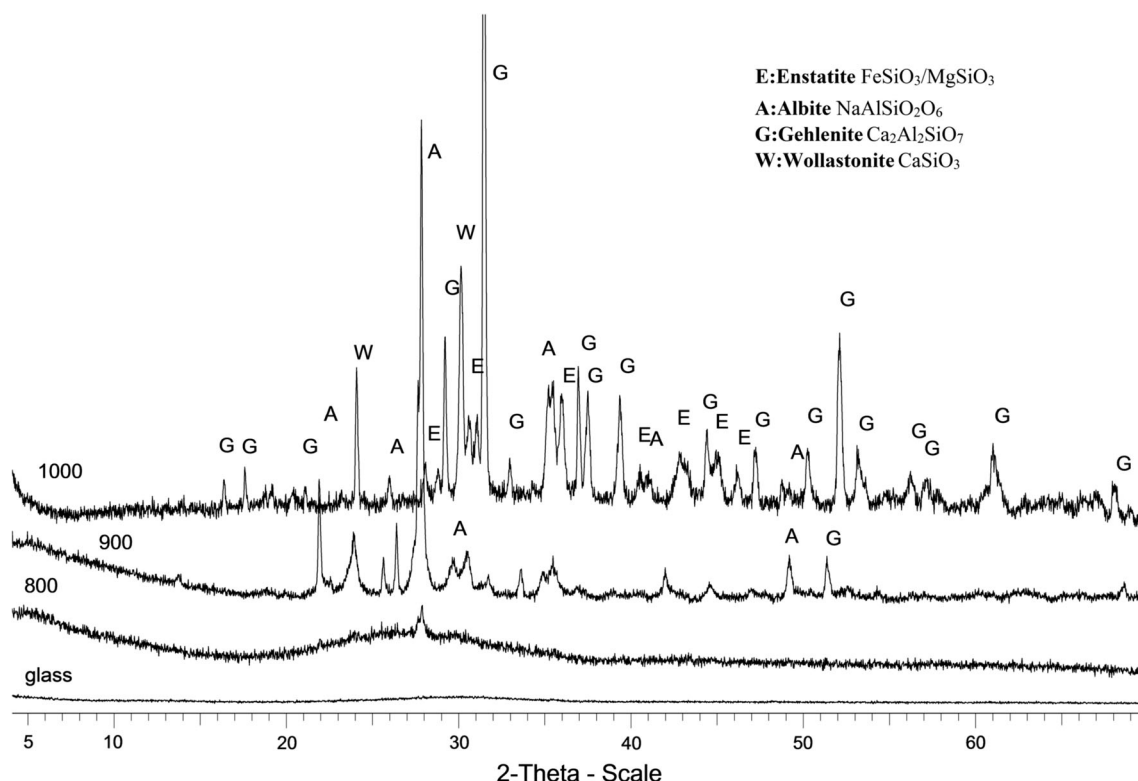


Fig. 4 XRD patterns of glass G-90P10RM and the produced glass–ceramic GC-90P10RM at 800, 900 and 1000 °C

EDS analysis confirms the presence of wollastonite (Fig. 5f) which is also identified in the respective XRD pattern. According to Erol et al. [46], Ca, Mg and Fe ions are considered as network modifiers that attract O^{2-} ions from the silicon tetrahedra $(SiO_4)^{4-}$ breaking the Si–O–Si bonds and forming different crystalline phases such as enstatite and wollastonite. In glass–ceramics GC-90P10SK produced after sintering of glass formed from fly ash and 10 % ferronickel slag, it is shown that spherical and laminar shaped grains are uniformly distributed within the glassy phase (Fig. 5g). In the same figure a denser microstructure with smaller pores can be also seen. Spherical particles varying in size from 2.5 to 5.5 μm correspond to enstatite (E) and laminar particles with a mean particle size of 5 μm to brownmillerite (B), as also indicated in the respective EDS analysis (Fig. 5h). The glassy phase consists mainly of compounds containing Na, Mg, Ca and Si (Fig. 5i).

Figure 6 shows two additional SEM images of glass–ceramics GC-90P10SK and GC-90P10RM produced after sintering at higher temperature, 1000 °C. Figure 6a indicates that the microstructure of the glass–ceramic GC-90P10SK is more dense compared to the one produced at a lower sintering temperature, 900 °C (Fig. 5g) and that the amount of the glassy phase was reduced. Finally, Fig. 6b shows very clearly the dendritic network of wollastonite crystals in GC-90P10RM.

Thermal Treatment of Glasses

The behaviour of the glass powder during heating was investigated through DTA, where glass transition (T_g) and crystallisation temperatures (T_c) were determined (Fig. 7). It is shown that in all samples T_g and T_c depend strongly on the composition of the raw materials. In glasses with high Fe content (G-50P50RM and G-90P10SK), namely 25 and 15 % respectively, the endothermic peaks at 600 and 700 °C indicate the glass transition temperature, while the exothermic peaks at 716 °C for the glass produced from slag and fly ash (G-90P10SK) are probably related to decomposition of calcite. The exothermic peaks around 850 °C, shown in both specimens, are also related to iron phase transformations.

For the glasses produced from raw materials with higher SiO_2 content (G-90P10SS), T_g is below 600 °C and T_c is 700 °C. Both temperatures were shifted to lower values and peaks became more intense when compared with the respective glasses produced from raw materials with high Fe_2O_3 content (G-50P50RM, G-90P10SK). In the latter case for the glass G-50P50RM T_g is around 700 °C and T_c at 900 °C while for the glass G-90P10SK T_g drops to 630 °C and T_c to 720 °C respectively. The higher glass transition and crystallization temperatures are also evident in G-90P10RM glass where T_g is 850 °C, and T_c is around 910 °C. This decreasing trend in temperature is also related

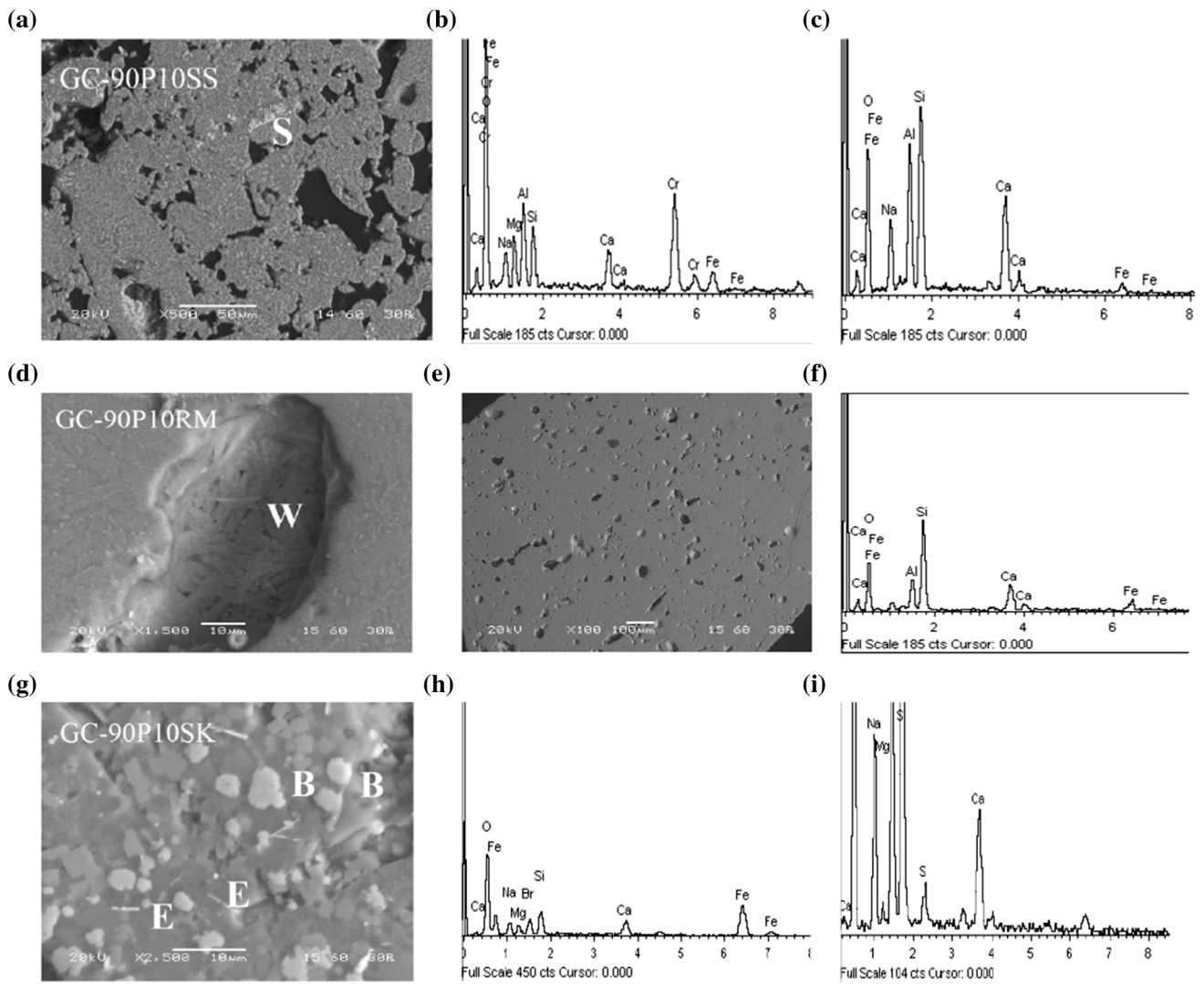


Fig. 5 SEM images and elemental spectrums (EDS analysis) of GC-90P10SS (a–c), GC-90P10RM (d–f) and GC-90P10SK (g–i) glass–ceramics produced after sintering glass powder at 900 °C

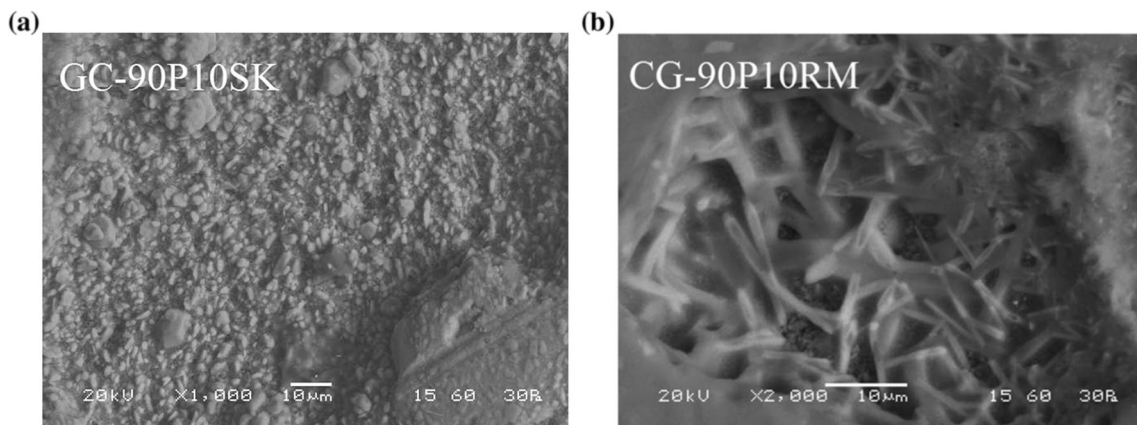


Fig. 6 SEM images of GC-90P10SK (a) and GC-90P10RM (b) glass–ceramics produced after sintering glass powder at 1000 °C

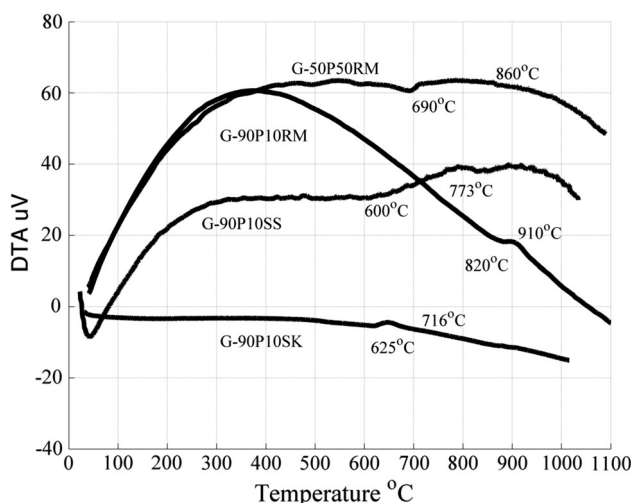


Fig. 7 DTA of glasses

to the initial particle size of the raw materials used for the synthesis of glasses which is around 30 μm for G-90P10SS and 80 μm for the coarser G-90P10RM. Based on the DTA results the sintering temperature for all glasses was decided to be 100 °C higher than glass transition temperature to ensure that sinter-crystallization is completed.

FTIR Analysis

Figures 8, 9, 10, and 11 present the FTIR spectra of raw materials, the produced glasses as well as the respective glass–ceramics produced at 900 °C. The identified FTIR bands are consistent with infrared data of commercial silicate glasses and glass–ceramics [14]. The spectra can be divided in three main regions, including high frequency bands between 1000 and 1100 cm⁻¹, many mid frequency bands between 480 and 700 cm⁻¹, and lower frequency and weaker bands up to 2000 cm⁻¹. The intensity of the peaks of the produced glass–ceramics varies depending on the glass composition.

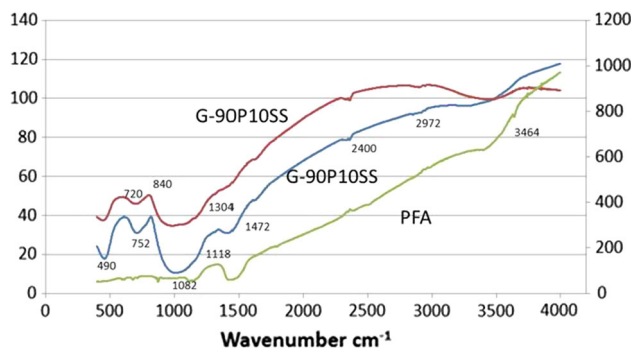


Fig. 8 FTIR spectra of Ptolemais fly ash, G-90P10SS glass and GC-90P10SS glass–ceramic

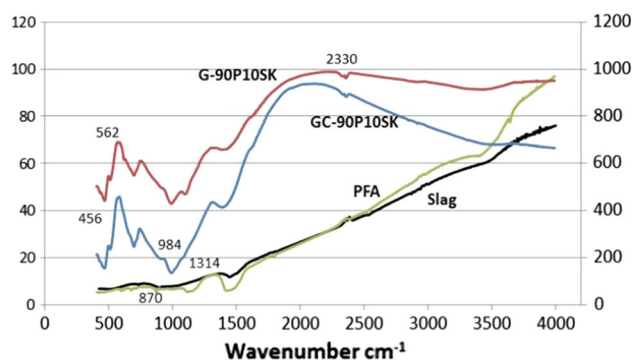


Fig. 9 FTIR spectra of Ptolemais fly ash, slag, G-90P10SK glass and GC-90P10SK glass–ceramic

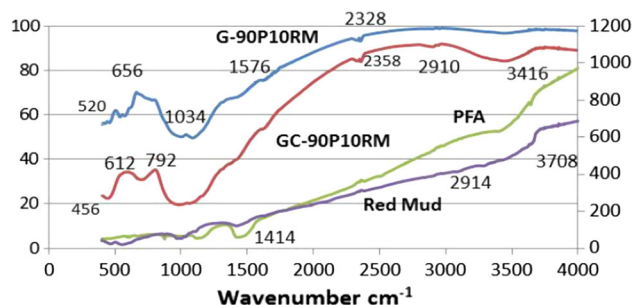


Fig. 10 FTIR spectra of Ptolemais fly ash, red mud, G-90P10RM glass and GC-90P10RM glass–ceramic

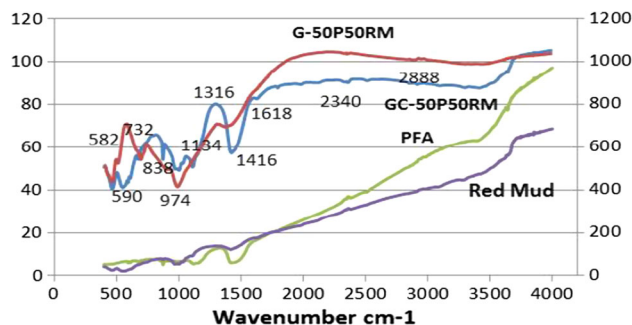


Fig. 11 FTIR spectra of Ptolemais fly ash, red mud, G-50P50RM glass, and GC-50P50RM glass–ceramic

Peaks in glasses containing low SiO₂ and high Al₂O₃ and CaO content as well as in the respective glass–ceramics become weaker in high and mid frequency bands, while at low frequency bands show higher intensity [47]. The band seen at 480⁻¹ cm in all glasses can be attributed to the bending motions of the aluminosilicates and the formation of Fe phases. Peak intensity is stronger for glasses with high Si/Al ratio such as the G-90P10SS. A doublet of peaks between 600 and 800 cm⁻¹ is mainly due to Si–O–Si symmetric stretching of bridging oxygen between SiO₄ tetrahedra. The band at around 1000 cm⁻¹ is attributed to asymmetric stretching vibrations of the silicate tetrahedral network. The strong band seen at around

1400 cm^{-1} is more dominant for glass–ceramics with high Ca content like GC-50P50RM and is due to atmospheric carbonation, asymmetric stretching and out of plane bending modes of CO_3 contained in CaCO_3 [48].

Weaker bands shown mostly in glass–ceramics at 2400 cm^{-1} are probably due to the presence of Fe phases. Peak intensity gets stronger as Fe content increases and this is evident for glass–ceramics produced after sintering of glasses containing fly ash, red mud and slag (GC-50P50RM, GC-90P10SK). Finally, small bands seen at 3600 cm^{-1} are associated to stretching vibrations of the –OH bond or to the presence of silanol (SiOH) [49]. FTIR results of the present study confirm the silicate glass–ceramics structure [50, 51].

Properties of Glass–Ceramics

The open porosity and bulk density of glass–ceramics produced after sintering of glass powder at 800, 900 and 1000 °C, are presented in Table 4.

The results indicate that the increase of sintering temperature results in an increase of bulk density and a respective noticeable decrease of porosity for all glass–ceramics. During sintering of the glass powder, the pores develop intergrain contacts due to diffusion kinetics, thus resulting in densification of the final matrix and a further decrease in porosity. The better packing of particles, as also shown in the previous section describing microstructure through SEM analysis, results in a more homogeneous structure and a gradual decrease in porosity in the produced glass–ceramics. Sintering of powdered glasses, with a mean particle size of 20 μm , also results in better rearrangement of grains, faster diffusion kinetics and early densification. The well-developed crystalline structure of glass–ceramics was also observed in XRD patterns. However, glass–ceramics produced after sintering of glasses formed from fly ash and red mud, such as GC-90P10RM and GC-50P50RM with a CaO content higher than 20 %, exhibited higher porosity, ranging between 6 and 36 %; the highest value, 36.8 %, was determined at the lower sintering temperature. This trend in porosity was also observed in other studies where high residual porosity, around 30 %, was reported for glass–ceramics produced from fly ash, silica sand and metallurgical slag [15, 23, 28].

Both open porosity and bulk density of glass–ceramics are strongly affected by chemical composition, particle size and degree of crystallization of the raw materials used. The lower values of porosity, in the range of 2–4.1 %, were obtained for glass–ceramics, i.e. GC-90P10SS and GC-90P10SK, produced after sintering of glasses with high Si/Al ratio (Si/Al: 6.6) at 1000 °C. Figure 12a shows that particle size analysis of all glass–ceramics is similar. On the other hand the pore size distribution is very different between the glass–ceramics produced from glasses formed from slag and silica sand or red mud (Fig. 12b). The first ones (GC-90P10SK and GC-90P10SS) with mean pore sizes 3.7 μm and 24 μm , respectively, exhibit very low open porosity, while the others (GC-50P50RM and GC-90P10RM), with mean pore sizes 30 and 60 μm , respectively, are characterized by a bimodal pore size distribution and show a much higher porosity when the sintering temperature is between 900 and 1000 °C. These observations may be combined with the microstructure of these glass–ceramics as shown with SEM images, Figs. 5e, 6a.

Mechanical properties of glass–ceramics, namely compressive strength and Vickers microhardness, were also determined. The compressive strength of the produced glass–ceramics depends on the final microstructure which is affected by the sintering temperature and the particle size of the powdered glass. As the sintering temperature increases from 800 °C to 1000 °C porosity values decrease and the compressive strength shows a noticeable increase reaching 194 MPa for the glass–ceramics produced after sintering of glass formed from fly ash and 10 % w/w silica sand (90P10SS) (Table 5).

Vickers microhardness is also high for all glass–ceramics produced after sintering at 1000 °C. The maximum value, exceeding 730 HV, was obtained for glass–ceramic GC-90P10SS indicating that the presence of Si-phases in glass improves substantially both the mechanical and physical properties of the final products. According to He et al. [17], the increase in the CaO content in glasses results in an increase of both hardness and compressive strength of the produced glass–ceramics due to the crystallization of wollastonite which assists in the development of a homogeneous microstructure. This observation is in agreement with the results of the present study. Wollastonite is the dominant phase in glass–ceramic GC-90P10RM which

Table 4 Open porosity and bulk density of glass–ceramics

Glass–ceramic	Open porosity (%)			Bulk density (g/cm^3)		
	800 °C	900 °C	1000 °C	800 °C	900 °C	1000 °C
GC-50P50RM	36.7	11.3	6.5	1.8	1.9	1.9
GC-90P10RM	32.3	23.0	15.7	1.8	2.0	2.1
GC-90P10SS	31.4	2.4	2.0	1.8	2.4	2.4
GC-90P10SK	22.7	4.1	2.6	2.2	2.3	2.4

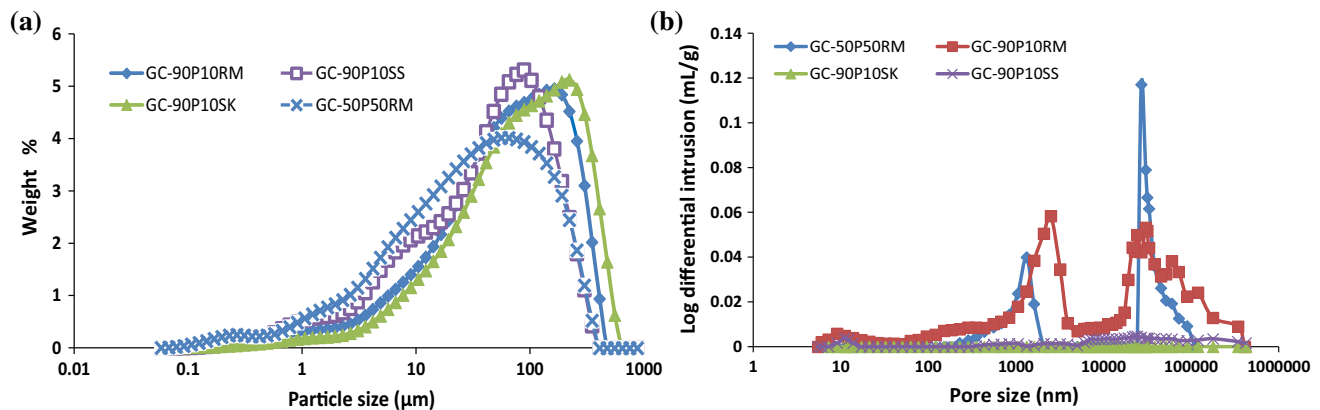


Fig. 12 **a** Laser particle size analysis and **b** pore size distribution (log differential intrusion vs. pore size) of glass–ceramics produced at 1000 °C

Table 5 Mechanical properties of glass–ceramics

Composition	Compressive strength (MPa)			Vickers microhardness (HV)			CTE 20–600 °C ($10^{-6}/\text{K}$)
	800 °C	900 °C	1000 °C	800 °C	900 °C	1000 °C	
GC-50P50RM	21	20	23	257	321	353	2.4
GC-90P10RM	16	49	72	380	447	524	2.8
GC-90P10SS	30	115	194	550	620	732	4.9
GC-90P10SK	10	30	58	584	614	704	1.8

exhibited high hardness and compressive strength, 524 HV and 72 MPa, respectively.

Increase in sintering temperature also resulted in higher hardness varying from 257 to 524 HV for specimens produced from glass formed from fly ash and red mud (GC-50P50RM, GC-90P10RM), and 550–732 HV for glass–ceramics produced from glass formed from fly ash, silica sand and slag (GC-90P10SS, GC-90P10SK).

Based on the values of porosity ($>23\%$), bulk density ($1.84\text{--}2.13\text{ gr/cm}^3$) and compressive strength (21–72 MPa), it is deduced that glass–ceramics produced from glass formed from fly ash and red mud (GC-50P50RM, GC-90P10RM) can be used as filters, catalytic materials and lightweight ceramics [11, 16, 17]. According to previous studies [29, 33, 50], open porosity higher than 30 %, high mechanical strength, narrow particle size distribution and high chemical resistance are required in order to use porous materials as filters and catalysts. On the contrary, glass–ceramics produced from silica sand (GC-90P10SS) and slag (GC-90P10SK) exhibiting higher density, lower porosity and high compressive strength may be used as construction materials. Leroy et al. [6] mentioned that recommended values of density, compressive strength and CTE for commercial bricks are $1.65\text{--}2.08\text{ g/cm}^3$, 4.8–27.6 MPa and $4.5\text{--}9 \times 10^{-6}/\text{K}$ respectively, while for building tiles the compressive strength should range between 26 and 44 MPa.

Dilatometric studies have been also performed and the CTE has been determined for the temperature range of

20–600 °C. As it is shown in Table 5, CTE values are considered relatively low, while the highest value of $4.91 \times 10^{-6}/\text{K}$ is obtained for glass ceramics produced from glass high alkali content, almost 10 % (GC-90P10SS). These values are consistent with the results obtained by Ribiero et al. [19], who also observed that the higher CTE are related to the presence of alkalis in the glassy phase.

In Table 6 the main properties of the glass–ceramics produced in the present study are compared with results presented in other studies indicating the high valorization potential of high calcium fly ash, low calcium ferronickel slag and red mud for the production of glass–ceramics with properties suitable for a number of applications.

Potential Toxicity of Glass–Ceramics

The TCLP results of the raw materials and the produced glass–ceramics after sintering of glass at 900 °C, in terms of Cr and Ni which show noticeable leachability in the raw materials, namely fly ash and slag respectively, are presented in Table 7. The leachability of other elements such as Cu, Zn, Cd and Pb was also determined but all values measured were below detection limit for both raw materials and glass–ceramics produced.

Table 7 shows that the leachability for both Ni and Cr in the produced glass–ceramics is either below detection limit or negligible. The highest concentration, 2.81 mg/L Cr, is shown for the GC-90P10SK glass–ceramic, which is

Table 6 Comparison of properties of various glass–ceramics

Raw material	Crystallization temperature (°C)	Compressive strength (MPa)	Density (g/cm ³)	Porosity (%)	Reference
Fly ash	1150–1200		1.93–3.19	0.3–15	[8]
Fly ash, waste glass	950–1100	26–76	1.6–2.2		[12]
Fly ash, silica sand	750–950	65–70 (bending strength)	2.9–3		[15]
Aluminum waste, waste glass, clay, peat ash	1080–1180	32–42	2.5–2.94		[52]
Slag, kaolin, quartz	1200–1220	3–28	2.1–2.34	39–49	[18]
Fly ash, red mud, silica sand	910–950		2.8–2.9	6–10	[46]
Fly ash, slag, silica sand, clay	900–1200	20–73	1.8–2.68	5–35	[22]
Fly ash, red mud, slag, silica sand	800–1100	10–115	1.8–2.35	2–36	Present study

though well below the respective TCLP limit of 5 mg/L. No TCLP limit is available for Ni.

The substantial decrease of leachability of heavy metals in glass–ceramics is mainly attributed to the increase in the degree of crystallinity and the entrapment of heavy metal ions in a well-developed structure [15, 20, 53].

Structural Integrity of Glass–Ceramics

It is anticipated that the chemical stability of the produced glass–ceramics will depend on the degree of crystallinity and microstructure. The % weight loss of glass–ceramics produced after sintering at 900 °C, after immersion in distilled water (pH 6.5), simulated acid rain (pH 3) and seawater (pH 8.2) for 1, 7 and 30 days is shown in Table 8. The results indicate that immersion for a period longer than 7 days does not result in any further noticeable increase in weight loss for all glass–ceramics and solutions tested. The highest weight loss, as anticipated, was recorded for specimens immersed in simulated acid rain solution, which simulates a highly corrosive environment. The slightly higher weight loss of glass–ceramics immersed in sea water, compared to distilled water, is attributed to the effect of chlorine ions present in seawater [54].

Glass–ceramics produced from glasses formed from raw materials containing fly ash and red mud (GC-90P10RM, GC-50P50RM and GC-90P10SK), exhibited lower chemical resistance and this is probably due to the gelatinization of gehlenite in acidic solutions [19]. The weight loss recorded is mainly attributed to the dissolution of the glassy phase.

Table 9 shows the compressive strength and the weight loss of glass–ceramics subjected to two 48 h freeze–thaw cycles, using –10 and 80 °C as temperature extremes, according to ASTM standard C1262-10 [55].

Results show that weight loss is limited for all glass–ceramics tested and varies between 0.6 and 4.1 %. On the other hand, the loss of compressive strength is rather low for glass–ceramics produced after sintering of glass produced from raw materials containing fly ash and either silica sand or slag (GC-90P10SS and GC-90P10SK). The first specimen maintained its compressive strength in remarkable levels (106 MPa). Finally, glass–ceramics produced from glasses formed from fly ash and red mud (GC-50P50RM, GC-90P10RM), exhibited limited weight loss (3.1–4.1 %), but considerable loss of compressive strength which varied between 22.4 and 25 %.

Conclusions

Glass–ceramics with beneficial properties can be successfully produced through sintering of glasses deriving from industrial wastes such as high calcium fly ash, low calcium ferronickel slag and red mud.

The main crystalline phases detected in glass–ceramics were wollastonite, spinel (chromite), enstatite and diopside. A small amount of glassy phase remained in the matrix at 900 °C, while sintering at 1000 °C results in an increase of crystallinity and intensity of peaks associated mainly with Ca and Fe phases. Crystal particles of 2–5.5 µm were

Table 7 Concentration of heavy metals (mg/L) in the TCLP extract of raw materials and glass–ceramics produced after sintering at 900 °C

Element	GC-50P50RM	GC-90P10RM	GC-90P10SS	GC-90P10SK	Slag	Fly ash	Red mud	US EPA limit
Cr	0.25	<DL	0.77	2.81	<DL	678.9	<DL	5
Ni	0.09	0.21	0.18	<DL	429.5	<DL	<DL	–

DL detection limit

Table 8 Weight loss (%) of glass–ceramics produced after sintering at 900 °C after immersion in different solutions

Glass–ceramic	Distilled water			Simulated acid rain			Seawater		
	1d	7d	30d	1d	7d	30d	1d	7d	30d
	GC-50P50RM	1.70 (±0.6)	1.77 (±0.81)	2.84 (±0.42)	4.78 (±0.44)	5.27 (±1.84)	6.06 (±1.06)	3.02 (±0.43)	4.33 (±0.14)
GC-90P10RM	2.14 (±0.71)	2.22 (±0.78)	3.33 (±0.92)	8.49 (±0.70)	8.99 (±1.60)	9.96 (±1.34)	4.14 (±0.50)	5.23 (±0.17)	7.17 (±0.63)
GC-90P10SS	0.88 (±0.06)	0.92 (±0.95)	0.98 (±0.33)	2.78 (±0.96)	3.39 (±1.84)	4.16 (±0.75)	1.27 (±0.83)	1.44 (±0.92)	1.56 (±0.23)
GC-90P10SK	0.97 (±0.05)	1.12 (±0.39)	2.01 (±0.08)	3.61 (±0.87)	4.15 (±0.95)	5.04 (±0.72)	1.87 (±0.41)	2.42 (±0.53)	2.97 (±0.92)

Table 9 Weight loss and compressive strength of glass–ceramics produced after sintering at 900 °C, according to ASTM standard C1262-10 [37]

Glass–ceramic	Weight loss (%)	Initial compressive strength (MPa)	Final compressive strength (MPa)	Compressive strength loss (%)
GC-50P50RM	4.1	20	15	25.0
GC-90P10RM	3.1	49	38	22.4
GC-90P10SS	0.6	115	106	7.8
GC-90P10SK	2.0	30	26	13.3

uniformly dispersed into the glassy matrix in all glass–ceramics as indicated by the use of analytical techniques.

Sintering temperature and initial glass compositions are considered as the main factors that affect the final properties of the glass–ceramics. Sintering temperature affects porosity, microhardness, compressive strength and linear thermal expansion coefficient. Also, the increase of sintering temperature results in increase of density, for which the maximum values (2.4 g/cm³) were acquired for glass–ceramics produced from fly ash and silica sand or slag. Glass–ceramics prepared from red mud and fly ash, with CaO content higher than 20 %, show higher porosity which reaches 36.7 %. Despite the increase of porosity, the compressive strength and the Vickers microhardness of all glass–ceramics are high reaching 194 MPa and 732 HV, respectively, for specimen GC-90P10SS, which was produced after sintering of glass at 1000 °C. Low thermal expansion coefficients, in the range of 1.8–4.9 × 10⁻⁶/K, have been also determined. Limited weight loss after immersing glass–ceramics in different solutions, including distilled water, seawater and even simulated acid rain, or subjecting them to freeze–thaw cycles and low or negligible concentration of heavy metals in TCLP extracts indicated their feasibility for potential applications in the construction sector.

Future work will focus on lowering the sintering temperature with the addition of fluxes or other wastes as well as on utilizing metallurgical slags and mining wastes, including nickel and gold wastes, for the production of glass–ceramics and ceramic foams. Emphasis will be given on the use of analytical techniques to characterise the microstructure and assess the anticipated properties of the final materials. Finally, the stabilization of hazardous mining and metallurgical wastes in a glass–ceramics matrix will be further investigated.

Acknowledgments This research has been co-funded by the European Union (European Social Fund) and Greek National Resources through the Operational Program “Education and Lifelong Learning” of the National Strategic Reference Framework (NSRF)—Research Funding Program: THALES, Sub-project “Development of

an integrated methodology for the management, treatment and valorisation of hazardous waste (WasteVal)” (code MIS 380038). Investing in knowledge society through the European Social Fund. The authors would also like to thank three anonymous reviewers for their constructive comments that improved the quality of the manuscript.

References

- Ghisellini, P., Cialani, C., Ulgiati, S.: A review on circular economy: the expected transition to a balanced interplay of environmental and economic system. *J. Clean. Prod.* (2015). doi:[10.1016/j.jclepro.2015.09.007](https://doi.org/10.1016/j.jclepro.2015.09.007)
- Ponsot, I., Bernardo, E., Bontempi, E., Depero, L., Detsch, R., Chinnam, R.K., Boccaccini, A.R.: Recycling of pre-stabilized municipal waste incinerator fly ash and soda-lime glass into sintered glass-ceramics. *J. Clean. Prod.* **89**, 224–230 (2015)
- Ljatifi, E., Kamusheva, A., Grozdanov, A., Paunović, P., Karamanov, A.: Optimal thermal cycle for production of glass-ceramic based on wastes from ferrometallurgy. *Ceram. Int.* **41**(9), 11379–11386 (2015)
- Yilmaz, G.: Structural characterization of glass-ceramics made from fly ash containing $\text{SiO}_2\text{-Al}_2\text{O}_3\text{-Fe}_2\text{O}_3\text{-CaO}$ and analysis by FT-IR-XRD-SEM methods. *J. Mol. Struct.* **1019**, 37–42 (2012)
- Zhao, Y., Chen, D., Bi, Y., Long, M.: Preparation of low cost glass-ceramics from molten blast furnace slag. *Ceram. Int.* **38**(3), 2495–2500 (2012)
- Leroy, C., Ferro, M.C., Monteiro, R.C.C., Fernandes, M.H.V.: Production of glass-ceramics from coal ashes. *J. Eur. Ceram. Soc.* **21**, 195–202 (2001)
- Zhang, J., Dong, W., Li, J., Qiao, L., Zheng, J., Sheng, J.: Utilization of coal fly ash in the glass-ceramic production. *J. Hazard. Mater.* **149**, 523–526 (2007)
- Erol, J.M., Kucukbayrak, S., Ersoy-Mericboyu, A.: Comparison of the properties of glass, glass-ceramic and ceramic materials produced from coal fly ash. *J. Hazard. Mater.* **153**, 418–425 (2008)
- Erol, J.M., Genc, A., Ovecoglu, M.L., Yucelen, E., Kucukbayrak, S., Taptik, Y.: Characterization of a glass-ceramic produced from thermal power plant fly ash. *J. Eur. Ceram. Soc.* **20**, 2209–2214 (2000)
- Wang, S., Zhang, C., Chen, J.: Utilization of coal fly ash for the production of glass-ceramics with unique performances: a brief review. *J. Mater. Sci. Technol.* **30**(12), 1208–1212 (2014)
- Shao, H., Liang, K., Zhou, F., Wang, G., Peng, F.: Characterization of cordierite-based glass-ceramics produced from fly ash. *J. Non Cryst. Solids* **337**, 157–160 (2004)
- Lu, J., Lu, Z., Peng, C., Li, X., Jiang, H.: Influence of particle size on sinterability, crystallization kinetics and flexural strength of wollastonite glass-ceramics from waste glass and fly ash. *Mater. Chem. Phys.* **148**, 449–456 (2014)
- Rincón, J.Ma., Romero, M., Boccaccini, A.R.: Microstructural characterization of a glass and a glass-ceramic obtained from municipal incinerator fly ash. *J. Mater. Sci.* **34**, 4413–4423 (1999)
- Cheng, W., Chen, Y.S.: On formation of $\text{CaO-Al}_2\text{O}_3\text{-SiO}_2$ glass-ceramics by vitrification of incinerator fly ash. *Chemosphere* **51**, 817–824 (2003)
- Yang, J., Xiao, B., Boccaccini, A.R.: Preparation of low melting temperature glass-ceramics from municipal waste incineration fly ash. *Fuel* **88**, 1275–1280 (2009)
- Cheng, T.W., Ueng, T.H., Chen, Y.S., Chiu, J.P.: Production of glass-ceramic from incinerator fly ash. *Ceram. Int.* **28**, 779–783 (2002)
- He, F., Tian, S., Xie, J., Liu, X., Zhang, W.: Research on microstructure and properties of yellow phosphorous slag glass ceramics. *J. Mater. Chem. Eng.* **1**, 27–31 (2013)
- Karamanova, E., Avdeev, G., Karamanov, A.: Ceramics from blast furnace slag, kaolin and quartz. *J. Eur. Ceram. Soc.* **31**, 989–998 (2011)
- Ribeiro, M.J., Labrincha, J.A.: Properties of sintered mullite and cordierite pressed bodies manufactured using Al-rich anodising sludge. *Ceram. Int.* **34**, 593–597 (2008)
- Cetin, S., Marangoni, M., Bernardo, E.: Lightweight glass-ceramic tiles from the sintering of mining tailings. *Ceram. Int.* **41**, 5294–5300 (2015)
- Tang, B., Lin, J., Qian, S., Wang, J., Zhang, S.: Preparation of glass-ceramic foams from the municipal solid waste slag produced by plasma gasification process. *Mater. Lett.* **128**, 68–70 (2014)
- Binhussain, M.A., Marangoni, M., Bernardo, E., Colombo, P.: Sintered and glazed glass-ceramics from natural and waste raw materials. *Ceram. Int.* **40**, 3543–3551 (2014)
- Loiseau, P., Caurant, D., Baffier, N., Mazerolles, L., Fillet, C.: Glass-ceramic nuclear waste forms obtained from $\text{SiO}_2\text{-Al}_2\text{O}_3\text{-CaO-ZrO}_2\text{-TiO}_2$ glasses containing lanthanides (Ce, Nd, Eu, Gd, Yb) and actinides (Th): study of internal crystallization. *J. Nucl. Mater.* **335**(1), 14–32 (2004)
- Amoroso, J., Marra, J.C., Tang, M., Lin, Y., Chen, F., Su, D., Brinkman, K.S.: Melt processed multiphase ceramic waste forms for nuclear waste immobilization. *J. Nucl. Mater.* **454**(1–3), 12–21 (2014)
- Yang, M., Guo, Z., Deng, Y., Xing, X., Qiu, K., Long, J., Li, J.: Preparation of $\text{CaO-Al}_2\text{O}_3\text{-SiO}_2$ glass ceramics from coal gangue. *Int. J. Miner. Process.* **102–103**, 112–115 (2012)
- Lu, Z., Lu, J., Li, X., Shao, G.: Effect of MgO addition on sinterability, crystallization kinetics, and flexural strength of glass-ceramics from waste materials. *Ceram. Int.* (2015). doi:[10.1016/j.ceramint.2015.10.142](https://doi.org/10.1016/j.ceramint.2015.10.142)
- Zhang, Z., Zhang, L., Li, A.: Remedial processing of oil shale fly ash (OSFA) and its value-added conversion into glass-ceramics. *Waste Manage.* **46**, 316–321 (2015)
- Ponsot, I., Bernardo, E.: Self glazed glass-ceramic foams from metallurgical slag and recycled glass. *J. Clean. Prod.* **59**, 245–250 (2013)
- Dong, Y., Zhou, J.E., Lin, B., Wang, Y., Wang, S., Miao, L., Lang, Y., Liu, X., Meng, G.: Reaction-sintered porous mineral based mullite ceramic membrane supports made from recycled materials. *J. Hazard. Mater.* **172**, 180–186 (2009)
- Banijamali, S., Aghaei, A.R.: Eftekhari Yekta, B.: Improving glass-forming ability and crystallization behavior of porous glass-ceramics in $\text{CaO-Al}_2\text{O}_3\text{-TiO}_2\text{-P}_2\text{O}_5$ system. *J. Non Cryst. Solids* **356**(31–32), 1569–1575 (2010)
- Hatcher, J., Pascual, M.J., Poulidi, D., Metcalfe, I.S.: Development and testing of an intermediate temperature glass sealant for use in mixed ionic and electronic conducting membrane reactors. *Solid State Ionics* **181**(15–16), 767–774 (2010)
- Chinnam, R.K., Francis, A.A., Will, J., Bernardo, E., Boccaccini, A.R.: Review. Functional glasses and glass-ceramics derived from iron rich waste and combination of industrial residues. *J. Non Cryst. Solids* **365**, 63–74 (2013)
- Reichelt, E., Heddrich, M.P., Jahn, M., Michaelis, A.: Fiber based structured materials for catalytic applications. *Appl. Catal. A* **476**, 78–90 (2014)
- Cao, J.K., Li, X.M., Wang, Z.X., Wei, Y.L., Chen, L.O., Guo, H.: Optical thermometry based on up-conversion luminescence behavior of self-crystallized $\text{K}_3\text{YF}_6\text{:Er}^{3+}$ glass ceramics. *Sens. Actuators B. Chem.* (2015). doi:[10.1016/j.snb.2015.10.087](https://doi.org/10.1016/j.snb.2015.10.087)
- Chen, D., Wan, Z., Zhou, Y., Ji, Z.: Cr³⁺-doped gallium-based transparent bulk glass ceramics for optical temperature sensing. *J. Eur. Ceram. Soc.* **35**(15), 4211–4216 (2015)
- Chen, D., Wan, Z., Zhou, Y., Huang, P., Zhong, J., Ding, M., Xiang, W., Liang, X., Ji, Z.: Bulk glass ceramics containing

- Yb³⁺/Er³⁺: β -NaGdF₄ nanocrystals: phase-separation-controlled crystallization, optical spectroscopy and upconverted temperature sensing behavior. *J. Alloys Comp.* **638**, 21–28 (2015)
37. Barbieri, L., Lancellotti, I., Manfredini, T., Queralt, I., Rincon, J.M., Romero, M.: Design, obtainment and properties of glasses and glass–ceramics from coal fly ash. *Fuel* **78**, 271–276 (1999)
 38. Rozenstrauha, I., Lodins, E., Krage, L., Drille, M., Balode, M., Putna, I., Filipenkov, V., Chinnam, R.K., Boccaccini, A.R.: Functional properties of glass–ceramic composites containing industrial inorganic waste and evaluation of their biological compatibility. *Ceram. Int.* **39**(7), 8007–8014 (2013)
 39. Francis, A.A., Abdel Rahman, M.K., Daoud, A.: Processing, structures and compressive properties of porous glass–ceramic composites prepared from secondary by-product materials. *Ceram. Int.* **39**, 7089–7709 (2013)
 40. Mymrin, V., Ribeiro, R.A.C., Alekseev, K., Zelinskaya, E., Tolmacheva, N., Catai, R.: Environment friendly ceramics from hazardous industrial wastes. *Ceram. Int.* **40**(7), 9427–9437 (2014)
 41. USEPA (US Environmental Protection Agency): Toxicity Characteristics Leaching Procedure (TCLP). Method 1311, Revision 0 (1990)
 42. Hirabayashi, D., Yoshikawa, T., Mochizuki, K., Suzuki, K., Sakai, Y.: Formation of brownmillerite type calcium ferrite (Ca₂Fe₂O₅) and catalytic properties in propylene combustion. *Catal. Lett.* **110**(3–4), 269–271 (2006)
 43. Sánchez-Ramos, S., Doménech-Carbó, A., Gimeno-Adelantado, J.V., Peris-Vicente, J., Valle-Algarra, F.M.: Thermal decomposition of chromite spinel with chlorite admixture. *Thermochim. Acta* **476**(1–2), 11–19 (2008)
 44. Ilic, M., Cheeseman, C., Sollars, C., Knight, J.: Minerology and microstructure of sintered lignite coal fly ash. *Fuel* **82**(30), 331–336 (2003)
 45. Xu, G.R., Zou, J.L., Li, G.B.: Stabilization of heavy metals in sludge ceramics. *Water Res.* **44**, 2930–2938 (2010)
 46. Erol, J.M., Kucukbayrak, S., Ersoy-Mericboyu, A.: The influence of the binder on the properties of sintered glass–ceramics produced from industrial wastes. *Ceram. Int.* **35**, 2609–2617 (2009)
 47. Atalay, S., Adiguzel, H.I., Atalay, F.: Infrared absorption study of Fe₂O₃–CaO–SiO₂ glass ceramics. *Mater. Sci. Eng., A* **304–306**, 796–799 (2001)
 48. Zaharaki, D., Komnitsas, K., Perdikatsis, V.: Use of analytical techniques for identification of inorganic polymer gel composition. *J. Mater. Sci.* **45**, 2715–2724 (2010)
 49. Komnitsas, K., Zaharaki, D., Perdikatsis, V.: Effect of synthesis parameters on the compressive strength of low-calcium ferronickel slag inorganic polymers. *J. Hazard. Mater.* **16**, 760–768 (2009)
 50. Liao, Q., Wang, F., Kuiru, C., Sheqi, P., Hanzhen, Z., Mingwei, L., Jianfa, Q.: FTIR spectra and properties of iron borophosphate glasses containing simulated nuclear waste. *J. Mol. Struct.* **1092**, 187–191 (2015)
 51. Nanko, M., Komarneni, S., Ishizaki, K.: *Porous Materials, Process Technology and Applications*, pp. 3–5. Kluwer Academic Publishers, London (1998)
 52. Lodins, E., Rozenstrauha, I., Krage, L., Lindina, L., Drille, M., Filipenkov, V., Chatzitheodoridis, E.: Characterization of glass–ceramics microstructure, chemical composition and mechanical properties. *Mater. Sci. Eng.* **25**, 1–10 (2011)
 53. Vu, D.-H., Wang, K.-S., Nam, B.X., Bac, B.-H., Tien-Chun Chu, T.-C.: Preparation of humidity-controlling porous ceramics from volcanic ash and waste glass. *Ceram. Int.* **37**(7), 2845–2853 (2011)
 54. Komnitsas, K., Zaharaki, D., Perdikatsis, V.: Geopolymerisation of low calcium ferronickel slags. *J. Mater. Sci.* **42**(9), 3073–3082 (2007)
 55. ASTM C1262-10 Standard Test Method for Evaluating the Freeze-Thaw Durability of Dry-Cast Segmental Retaining Wall Units and Related Concrete Units. ASTM International, West Conshohocken, PA. www.astm.org. Accessed 3 Aug 2015 (2010)